A Novel Recovery Strategy to Suppress Subsequent Commutation Failure in an LCC-Based HVDC

Changsheng Su, Chunya Yin, *Member*, *IEEE*, Fengting Li, and Lu Han

***Abstract*—A subsequent commutation failure (SCF) can easily occur during the recovery process after a first commutation failure (1st CF). This paper analyzes the interaction mechanism of extinction angle, AC voltage, DC current and firing angle, and reveals that the complex coupling relationship during the dynamic process after the 1st CF has a significant effect on the SCF. The mathematical equations when considering different fault durations, fault severities and AC system strengths are then established. An AC fault voltage detection method based on reactive power and fault duration is also proposed to measure the fault severity, and an SCF inhibition control strategy (SCFICS) based on AC fault detection and reactive power control is subsequently proposed. This can not only inhibit the SCF, but also enhance the DC recovery speed effectively. Finally, based on the SCFICS, a simulation model is built, and the simulation results with different cases indicate that the SCFICS can effectively inhibit the SCF with good recovery performance, for three-phase-to-ground (TPG) and single-phase-to-ground faults, and with a fault inductance range of 0.01 H to 1 H.**

***Index Terms*—Commutation failure, LCC-HVDC, reactive power, AC system fault, control strategies.**

I. Introduction

The line commutated converter (LCC) HVDC is widely used in large capacity and long-distance power transmission across regions all over the world [1]. However, because of the strong coupling between the AC and DC systems, an AC system fault can easily cause commutation failure (CF) of the inverter [2], [3]. After the 1st CF, during the recovery process, subsequent commutation failure (SCF) can also easily occur because of the interaction of electrical quantity and control quantity. Multiple-CFs may lead to DC blocking, and the risk of a cascading fault is high [4], [5]. Therefore, study on a suppression strategy of the SCF, also clarifying the mechanism of SCF, is key to preventing a cascading fault.

To date, much research has focused on the mechanism of and suppression strategy for the 1st CF. A mathematical model of extinction angle is proposed in [6], and that reveals that AC voltage drop and DC current rise are the main factors that affect CF. The influence of the harmonic and superconductive current limiter (SCL) on the CF is further analyzed in [7], [8]. A series of control strategies have been proposed to inhibit CF, based on the DC current predictive [9], SCF [10], fuzzy controller [11], advanced triggering [12], DC current limit [13], predictive controller [14] and overlap area real-time measurement [15].

At present, the mechanism and influencing factors of the 1st CF are clear, and the CF is an inherent property of thyristors due to the rapid dynamics of electrical and control quantity after AC faults. In addition, for the delay characteristic of the HVDC controller, the CF cannot be fully suppressed in the case of serious faults (deep voltage drop), while an improved HVDC controller can only reduce the probability of the 1st CF. Since an SCF generally occurs during the recovery process, the controller has not sufficient time to suppress the SCF, while the mechanism of SCF is different from that of the 1st CF. Hence, the influence factors of the two are also different, and the 1st CF suppression strategy cannot be directly applied to the SCF. A new CF recovery method and current limiter based on AC voltage are proposed in [16], [17]. However, the interactive coupling relationships among firing angle, DC current and AC voltage during the recovery process after the 1st CF are not considered. The SCF mechanism is unclear and the effect on the SCF suppression is not significant, and whether the controller with fixed parameters can be applied to the system with other parameters needs to be further discussed. Reference [18] analyzes and concludes that the control switching in the inverter is the main factor that affects the SCF and on this basis, by increasing the firing angle, an SCF strategy is proposed. However, the controllers of the CIGRE

Received: March 16, 2023
Accepted: October 28, 2023
Published Online: January 1, 2024
Chunya Yin (corresponding author) is with the School of Electrical Engineering, Xinjiang University, Urumqi 830017, China (e-mail: 1399132297@qq.com).
DOI: 10.23919/PCMP.2023.000203

HVDC system are different from actual HVDC systems, so the applicability of the proposed method to actual systems needs to be studied. Reference [19] proposes an SCF suppression strategy based on valve voltage real-time detection, although valve voltage detection requires high accuracy. Based on the HVDC output impedance through real-time detection of DC voltage and current, an SCF suppression strategy is proposed in [20], but the SCF mechanism is not discussed. An SCF early warning and suppression strategy based on increasing the firing angle is proposed in [21], but the simulation results show limited suppression effect. Reference [22] proposes an SCF suppression strategy by reducing the DC current order value during the recovery period, but it can lead to the problem of slow recovery speed. Reference [23] analyzes the influence of fault duration and severity, and SCR on the SCF. However, the mechanism analysis is simple and lacks a theoretical basis for SCF suppression strategy. In [24], the influence of firing angle deviation on the subsequent commutation failure is analyzed, and a dynamic adaptive compensation of the firing angle deviation method is proposed. A general self-adaptive DC current control method is proposed to eliminate the SCF in [25]. This can improve the dynamic reactive power support capability. In [26] and [27], a DC current limited method is proposed. While it can suppress SCF effectively, it also leads to a slow recovery.

The above review shows that previous research has mostly focused on SCF suppression strategies by reducing DC current or increasing firing angle. However, during the recovery process after the 1st CF, the dynamic changes and the coupling relationships of AC voltage, DC current, reactive power, fault severity, fault duration and firing angle have significant effects on the extinction angle, and thus how to clarify the mechanism and dominant factors of an SCF is the key to suppressing strategies.

The main contributions of this paper are:

1) Considering different fault durations, fault severities and AC system strengths, the mathematical expression of the converter bus voltage is established, and the main influencing factors on an SCF are clarified.

2) Considering the recovery speed and SCF suppression ability, a self-adaption SCF inhibition control strategy which can support the AC voltage is proposed.

This remainder of the paper is organized as follows. In Section II, the communication failure influencing factors are analyzed, and the main control strategies are introduced. In Section III, the interaction mechanism of the extinction angle, DC current, AC voltage, reactive power and firing angle is analyzed, and the SCF influence factors are obtained. In Section IV, an SCF inhibition control strategy (SCFICS) based on AC fault detection and reactive power control is proposed, while in Section V, the SCFICS is built with different cases. In Section VI, the applicability of the proposed method is discussed. Section VII concludes the paper.

II. Commutation Failure and Existing Control Strategies

A. Commutation Failure Influence Factors

The topological structure of a six-pulse inverter (Graetz Bridge) is shown in Fig. 1 [28].

In Fig. 1, U_{di} represents the DC Voltage at the inverter side; I_d represents the DC current; L_c represents commutation inductance; u_a, u_b, and u_c represent the instantaneous values of commutation voltage.

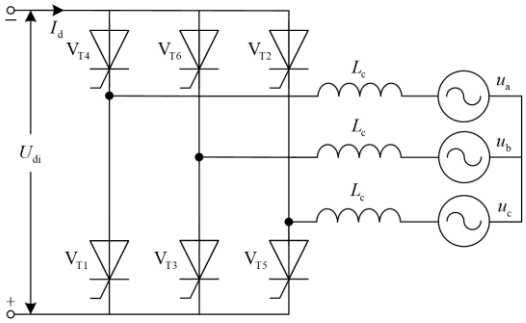

Fig. 1. The topological structure of a Graetz Bridge.

As can be seen in Fig.1, the inverter is composed of six valves ($V_{T1} - V_{T6}$), which are sequentially connected in a certain order. The thyristor is the basic component in the inverter, and to make the thyristor conduct, two conditions need to be met, i.e., a positive voltage and a firing pulse. However, to turn off a thyristor, a reverse voltage for a certain period (i.e., the extinction angle γ) is necessary. Meanwhile, because of L_c, the commutation process will take a finite time (i.e., the overlap angle μ).

From Fig. 1, Fig. A1 in the Appendix A depicts the commutation voltage, DC voltage, and valve voltage waveforms of the Graetz bridge. $P_1 - P_6$ is the firing pulse of the six thyristor valves. During the commutation process from V_{T2} to V_{T4}, because of L_c, V_{T2} cannot be turned off instantaneously, and hence, the valve voltage on V_{T2} remains at 0. When V_{T4} is completely conducting, as can be seen in Fig. A1, the valve voltage on V_{T2} is the line voltage (u_{ac}). Therefore, V_{T2} will withstand a negative voltage for a certain time (which is defined as the extinction angle, γ), and then the valve voltage on V_{T2} will turn positive.

If the valve is just withdrawn from conduction before it fails to regain its blocking capacity, the valve will turn on itself when the voltage applied on returns to positive. This is called commutation failure. Hence, for successfully turning off a valve, the time for the valve to withstand the reverse voltage needs to be greater than

the minimum time ($\gamma_{\min}$) required for the valve to turn off. Otherwise, commutation failure occurs.

The most commonly used extinction angle mathematical model can be expressed as [6]:

$$\gamma = \arccos(\frac{\sqrt{2}I_{\mathrm{d}}}{T_{\mathrm{i}}U_{\mathrm{Li}}}X_{\mathrm{ci}} + \cos\beta) \tag{1}$$

where U_{Li} represents the converter bus voltage of the inveter; β represents the advanced firing angle of the inverter; T_{i} represents transformation ratio at the inverter side; X_{ci} represents the commutation reactance of L_{c}, and X_{ci} can be expressed as [29]:

$$X_{\mathrm{ci}} = \frac{X_{\mathrm{ci,pu}}T_{\mathrm{i}}U_{\mathrm{LiN}}}{\sqrt{2}I_{\mathrm{dN}}} \tag{2}$$

where I_{dN} is the DC current at rated condition; U_{LiN} is the converter bus voltage at rated condition; $X_{\mathrm{ci,pu}}$ is the commutation reactance in per unit.

Based on (1) and (2), γ can be expressed as:

$$\gamma = \arccos(\frac{I_{\mathrm{d,pu}}}{U_{\mathrm{Li,pu}}}X_{\mathrm{ci,pu}} + \cos\beta) \tag{3}$$

where $I_{\mathrm{d,pu}}$ represents the DC current in per unit; and $U_{\mathrm{Li,pu}}$ represents the converter bus voltage in per unit.

As can be seen in (3), increasing I_{d} and decreasing U_{Li} will increase the CF risk.

B. Existing HVDC Control Strategies

In existing research, there are three commonly used control strategies at the inverter side [15], [30]: 1) ABB control strategies; 2) SIEMENS control strategies; and 3) CIGRE HVDC control strategies. The control structures of the three commonly used inverter control strategies are shown in Fig. 2.

In Fig. 2, α_{i} represents the firing angle of the inverter; $\alpha_{\max}$ and $\alpha_{\min}$ represent the maximum and minimum firing angle of the inverter respectively; γ_{ref} represents the reference value of the extinction angle; ΔU_{di}, ΔI_{di}, $\Delta\gamma$ represent the error of DC voltage, DC current and extinction angle, respectively.

As can be seen in Fig. 2, both the ABB and SIEMENS control strategies consist of three controllers: 1) extinction angel; 2) constant current; and 3) constant voltage. The difference between the ABB and SIEMENS control strategies is in the extinction angle controller, i.e., a predictive constant extinction angle control strategy (PCEA) is adopted in ABB, which can be expressed as:

$$\beta = \arccos(-\cos\gamma_{\mathrm{ref}} + \frac{\sqrt{2}X_{\mathrm{ci}}I_{\mathrm{d}}}{U_{\mathrm{Li}}} + k(I_{\mathrm{dref}} - I_{\mathrm{d}})) \tag{4}$$

where I_{dref} is the DC current order value; and k is a fixed parameter.

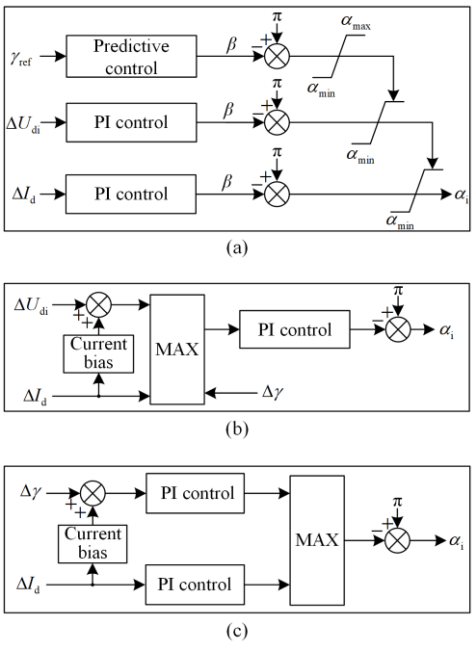

Fig. 2. Control structure diagram of inverter. (a) ABB control strategies. (b) SIEMENS control strategies. (c) CIGRE HVDC control strategies.

In the ABB control strategy, a commutation failure prevention (CFPREV) module is used. The main idea is to detect an AC fault quickly, so as to achieve the action of the controller in advance. However, it will result in an insufficiently accurate firing angle. For the SIEMENS and CIGRE control strategies, measured constant extinction angle (MCEA) control strategies are adopted. When γ is decreasing, the proportion integration (PI) controller will increase β to resist CF. However, the coupling relationships between electrical and control quantities are not considered.

In addition, the voltage-dependent current order limiter (VDCOL) is adopted. When the DC voltage is decreasing, the VDCOL will reduce the DC current. At present, almost all control strategies for inhibiting CF or CCF are based on Fig. 2, while the core idea is to increase β when the CF risk is detected. However, according to (3), U_{Li} and I_{d} will change dramatically during a transient process, and so will influence an SCF.

III. Subsequent Commutation Failure Influence Factors

A. The Interaction Mechanism of Extinction Angle, AC voltage, DC current and Firing angle

As smoothing reactors are configured at both ends of DC transmission lines, the DC current will not increase or decrease suddenly under a sudden change of DC voltage. The DC transmission line equivalent circuit is shown in Fig. 3 [31].

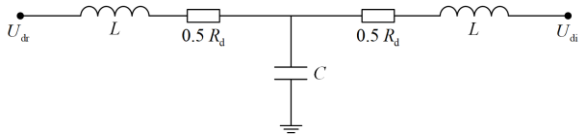

Fig. 3. The equivalent circuit of DC transmission line.

In Fig. 3, R_d is the equivalent resistance of the DC line; C is the equivalent capacitance of the DC line; L is the equivalent reactance of the smooth reactor; U_{dr} is the DC voltage at the rectifier side.

C has only a limited effect on the DC current, e.g., for the CIGRE HVDC Benchmark mode, C is only 26 μF. When C is ignored, according to Fig. 3, the DC current differential equation can be expressed as [32]:

$$2L\frac{\mathrm{d}I_d}{\mathrm{d}t}+I_dR_d=U_{dr}-U_{di}=\Delta U_d \tag{5}$$

From (5), I_d is:

$$I_d=\left(I_d(0\_)-\frac{U_{dr}-U_{di}}{R_d}\right)\mathrm{e}^{-\frac{R_d}{2L}t}+\frac{U_{dr}-U_{di}}{R_d} \tag{6}$$

In (6), ΔU_d has a significant effect on I_d. For a case with $I_d(0\_)=2$ kA, $R_d=5\,\Omega$, and $L=0.5$ H, the response curves of I_d with different ΔU_d are shown in Fig. 4.

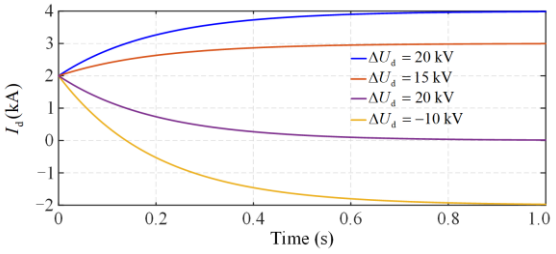

Fig. 4. The response curves of I_d with different ΔU_d.

As can be seen in Fig. 4, when $\Delta U_d>0$, I_d will increase nonlinearly with the increasing ΔU_d. When $\Delta U_d<0$, I_d will decrease nonlinearly with the decreasing ΔU_d.

U_{di} can be expressed as [33], [34]:

$$U_{di}=\frac{3\sqrt{2}}{\pi}NT_iU_{Li}\cos\beta+\frac{3}{\pi}NX_{ci}I_d \tag{7}$$

where N is the number of the six-pulse inverter.

Q_{di} can be expressed as [33], [34]:

$$Q_{di}=I_d\sqrt{U_{di0}^2-U_{di}^2} \tag{8}$$

where U_{di0} is the no-load DC voltage of the inverter; Q_{di} is the reactive power consumed by the inverter.

From (8), assuming that U_{di0} remains unchanged, $\mathrm{d}Q_{di}/\mathrm{d}t$ can be calculated as:

$$\frac{\mathrm{d}Q_{di}}{\mathrm{d}t}=\frac{\mathrm{d}I_d}{\mathrm{d}t}\sqrt{U_{di0}^2-U_{di}^2}-I_d\frac{U_{di}\dfrac{\mathrm{d}U_{di}}{\mathrm{d}t}}{\sqrt{U_{di0}^2-U_{di}^2}} \tag{9}$$

From (9), during the dynamic process, there is:

$$\frac{\mathrm{d}I_d}{\mathrm{d}t}\sqrt{U_{di0}^2-U_{di}^2}>I_d\frac{U_{di}\dfrac{\mathrm{d}U_{di}}{\mathrm{d}t}}{\sqrt{U_{di0}^2-U_{di}^2}} \tag{10}$$

Thus, for $\mathrm{d}Q_{di}/\mathrm{d}t>0$, Q_{di} increases, and it will lead U_{Li} to decrease, and thus the SCF risk increases.

To date, most control strategies for inhibiting CF are to increase β, as can be seen in (1), (6)–(8). However, there is a strong coupling relationship among γ, U_{Li}, β and I_d, e.g., although the increase of β can lead to γ increase directly, according (6) and (7), it will lead to U_{di} decrease and I_d increase, which will cause γ to decrease. Also, from (8), a Q_{di} increase will cause U_{Li} decrease, and consequent γ decrease. The compiling relationship is shown in Fig. 5.

Figure 5 depicts the coupling relationship among γ, U_{Li}, β and I_d, during the dynamic process after the 1st CF, and shows a complex and significant effect on γ. For different operational conditions, simply increasing or decreasing β may lead to an SCF.

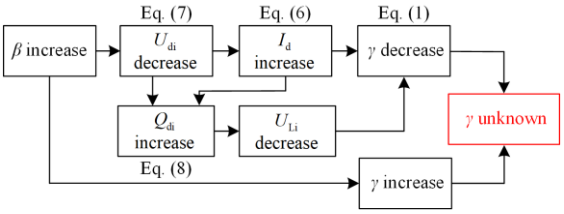

Fig. 5. Coupling relationship among γ, U_{Li}, β and I_d.

B. Subsequent Commutation Failure with Fault Duration and Fault Severity

To analyze the mechanism and influence factors of SCF, the recovery process needs further analysis.

As a decreasing U_{Li} is the significant reason for the CF, in order to analyze the trend of U_{Li}, we define t_f as the fault initiation time, t_{cf} as the CF duration, and t_{dur} as the fault duration.

Figure 6 depicts the simulation curves of $U_{Li,pu}$ in the event of a three-phase-to-ground (TPG) fault at $t_f=1$ s, with $L_f=0.5$ H and $t_{dur1}=0.1$ s, $t_{dur2}=0.15$ s, $t_{dur3}=0.2$ s.

As can be seen in Fig. 6, for $t_{dur1}=0.1$ s, only the 1st CF occurs (blue line), while for $t_{dur2}=0.15$ s and 0.2 s (green and red lines), an SCF occurs. Q_{di} will influence

$U_{\text{Li,pu}}$ during the whole dynamic process, while the influence of the fault on $U_{\text{Li,pu}}$ is related to t_{dur}.

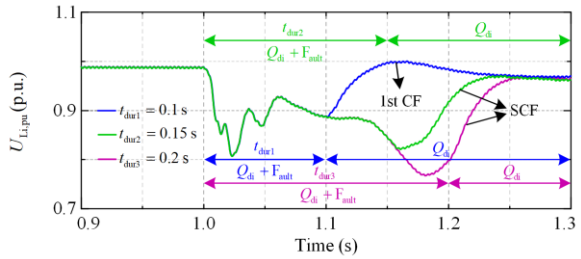

Fig. 6. The simulation curves of $U_{\text{Li,pu}}$ for a three-phase fault with different fault durations.

From the above analysis, for the different t_{dur}, $U_{\text{Li,pu}}$ can be expressed as:

$$U_{\text{Li,pu}} = \begin{cases} U_{\text{Lif,pu}} + \Delta U_{\text{LiQ,pu}}, & t \leqslant t_{\text{f}} + t_{\text{dur}} \\ 1 + \Delta U_{\text{LiQ,pu}}, & t > t_{\text{f}} + t_{\text{dur}} \end{cases} \tag{11}$$

where $U_{\text{LiQ,pu}}$, $U_{\text{Lif,pu}}$ are the converter bus voltage caused by reactive power and AC fault, respectively; $\Delta U_{\text{LiQ,pu}}$ is the transient overvoltage rise caused by reactive power.

To analyze the effect of fault duration and fault severity on an SCF, it is assumed that $t_{\text{dur2}} > t_{\text{dur1}} > t_{\text{cf}}$, i.e., t_{dur2} represents longer fault duration and t_{dur1} represents shorter fault duration. It also assumes $U_{\text{Li,pu1}} > U_{\text{Li,pu2}}$, i.e., $U_{\text{Li,pu1}}$ represents that the fault severity is less serious, and $U_{\text{Li,pu2}}$ represents that the fault severity is more serious. Based on this, the analysis of cases is shown in Table I and Fig. 7.

TABLE I
EVALUATION DATA AND RESULT (PORTION)

Cases	Fault severity	Fault duration	Lines in Fig. 7	
			$U_{\text{Li,pu}}$	U_{di}
1	$U_{\text{Li,pu1}}$	t_{dur1}	C1-F1-G1	D2-F2-G2-F2
2	$U_{\text{Li,pu1}}$	t_{dur2}	C1-J1-K1	D2-F2-K2-M2
3	$U_{\text{Li,pu2}}$	t_{dur1}	D1-E1-G1	D2-E2-H2-L2
4	$U_{\text{Li,pu2}}$	t_{dur2}	D1-H1-K1	D2-E2-J2-M2

In Fig. 7, during the 1st CF, U_{di} decreases to 0. For any cases in Table I, the recovery process of U_{di} after the 1st CF will go through two stages. One is from 0 to U_{di1} or U_{di2}, and the other is from U_{di1} or U_{di2} to U_{diN}. From (7), after a CF, in stage 1, U_{di} will recover to a fault steady state (U_{di1}) rapidly, and from (9), $\text{d}U_{\text{di}}/\text{d}t > 0$. As U_{di} increases rapidly, because of the delay time of the PI controller, the controller cannot act to adjust U_{dr} and I_{d} immediately, so I_{d} will decrease ($\text{d}I_{\text{d}}/\text{d}t < 0$). Since the change of I_{d} relies on the DC voltage and I_{dref} (DC current order value) is determined by the VDCOL, the change of I_{d} lags behind U_{di}. Therefore, in this stage, from (9), it will lead to $\text{d}Q_{\text{di}}/\text{d}t < 0$, and $U_{\text{Li,pu}}$ will not decrease.

For Case 1 in Table I, when the fault is not serious, $U_{\text{Li,pu}}$ will remain at a high value (U_{Li1}), and t_{dur} is not long (t_{dur1}). The change trend of $U_{\text{Li,pu}}$ can be seen as C1-F1-G1 in Fig. 7. During the time of [$t_{\text{f}} + t_{\text{cf}}$, $t_{\text{f}} + t_{\text{dur1}}$], assuming U_{di} remains unchanged (from point F2 to G2), $\text{d}U_{\text{di}}/\text{d}t = 0$ and I_{d} increases (i.e., $\text{d}I_{\text{d}}/\text{d}t > 0$) because of the I_{dref} increase. From (9), $\text{d}Q_{\text{di}}/\text{d}t > 0$, so the inverter will consume lots of reactive power, which will lead to an $U_{\text{Li,pu}}$ decrease in this stage. Consequently, $U_{\text{Li,pu}}$ will be smaller than $U_{\text{Li,pu1}}$, and the SCF risk will increase. With the increase of fault duration (when $t_{\text{dur}} = t_{\text{dur2}}$), for Cases 2 and 4 in [$t_{\text{f}} + t_{\text{cf}}$, $t_{\text{f}} + t_{\text{dur1}}$], because of the $U_{\text{Li,pu}}$ decrease, the SCF risk will further increase. For Case 3, for the serious fault, the lower $U_{\text{Li,pu}}$ ($U_{\text{Li,pu2}}$) will lead to a lower U_{di} (U_{di2}). Since $U_{\text{Li,pu}}$ is lower than $U_{\text{Li,pu2}}$, $U_{\text{Li,pu}}$ will decrease, and the influence of $U_{\text{Li,pu}}$ on the extinction angle is the main factor for the SCF.

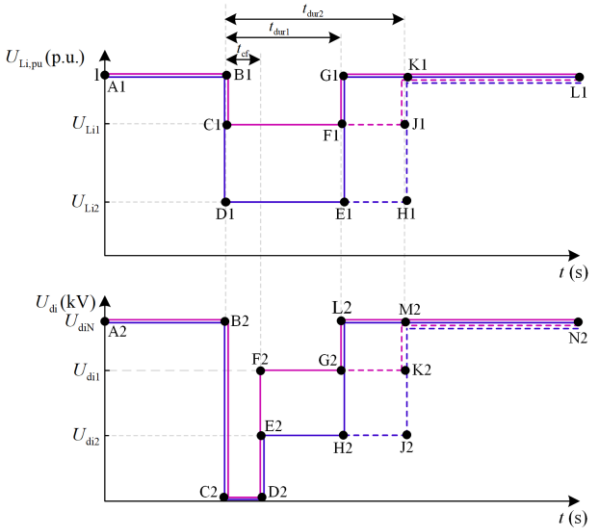

Fig. 7. The diagram of U_{Li} and U_{di} with different fault severities and fault durations.

C. Subsequent Commutation Failure with Reactive Power and AC System Strength

To quantitatively analyze the effect of Q_{di} on $U_{\text{Li,pu}}$ with different t_{dur} and $U_{\text{Lif,pu}}$, the relationship between $U_{\text{Li,pu}}$ and ΔQ_{i} can be expressed as [33]:

$$\Delta U_{\text{LiQ,pu}} = \frac{\Delta Q_{\text{i}}}{S_{\text{Ci}}} \tag{12}$$

where S_{Ci} is the short circuit capacity at the converter bus; ΔQ_{i} is the unbalanced reactive power between the AC and DC system, and can be expressed as:

$$\Delta Q_{\mathrm{i}} = U_{\mathrm{Li,pu}}^2 Q_{\mathrm{CiN}} - Q_{\mathrm{aciN}} - Q_{\mathrm{di}} \tag{13}$$

where Q_{aciN} is the reactive power exchange between the AC system and the inverter in rated power; and Q_{CiN} is the rated reactive power in the inverter station.

Substituting (13) into (12), $\Delta U_{\mathrm{LiQ,pu}}$ is:

$$\Delta U_{\mathrm{LiQ,pu}} = \frac{U_{\mathrm{Li,pu}}^2 Q_{\mathrm{CiN}} - Q_{\mathrm{aciN}} - Q_{\mathrm{di}}}{S_{\mathrm{Ci}}} \tag{14}$$

From (11), when $t \leqslant t_{\mathrm{f}} + t_{\mathrm{dur}}$, $U_{\mathrm{Li,pu}}$ is:

$$U_{\mathrm{Li,pu}} = \frac{U_{\mathrm{Li,pu}}^2 Q_{\mathrm{CiN}} - Q_{\mathrm{aciN}} - Q_{\mathrm{di}}}{S_{\mathrm{Ci}}} + U_{\mathrm{Lif,pu}} \tag{15}$$

Based on (15), $U_{\mathrm{Li,pu}}$ can be solved as:

$$U_{\mathrm{Li,pu}} = -\sqrt{\left(\frac{S_{\mathrm{Ci}}}{2Q_{\mathrm{CiN}}}\right)^2 - \frac{S_{\mathrm{Ci}} U_{\mathrm{Lif,pu}}}{Q_{\mathrm{CiN}}} + \frac{Q_{\mathrm{aciN}} + Q_{\mathrm{di}}}{Q_{\mathrm{CiN}}}} + \frac{S_{\mathrm{Ci}}}{2Q_{\mathrm{CiN}}} \tag{16}$$

When $t > t_{\mathrm{f}} + t_{\mathrm{dur}}$, combining (15) with (11), $U_{\mathrm{Li,pu}}$ is:

$$U_{\mathrm{Li,pu}} = -\sqrt{\left(\frac{S_{\mathrm{Ci}}}{2Q_{\mathrm{CiN}}}\right)^2 - \frac{S_{\mathrm{Ci}}}{Q_{\mathrm{CiN}}} + \frac{Q_{\mathrm{aciN}} + Q_{\mathrm{di}}}{Q_{\mathrm{CiN}}}} + \frac{S_{\mathrm{Ci}}}{2Q_{\mathrm{CiN}}} \tag{17}$$

As can be seen in (16), when $U_{\mathrm{Lif,pu}} = 1$ p.u., equation (16) is the same as (17). Then, for an AC/DC hybrid system with $S_{\mathrm{Ci}} = 3000$ MVA, $Q_{\mathrm{CiN}} = 540$ Mvar and $Q_{\mathrm{aciN}} = 0$, for different $U_{\mathrm{Lif,pu}}$, the relationship between $U_{\mathrm{Li,pu}}$ and Q_{di} is shown in Fig. 8, while for different Q_{di}, the relationship between $U_{\mathrm{Li,pu}}$ and $U_{\mathrm{Lif,pu}}$ is shown in Fig. 9.

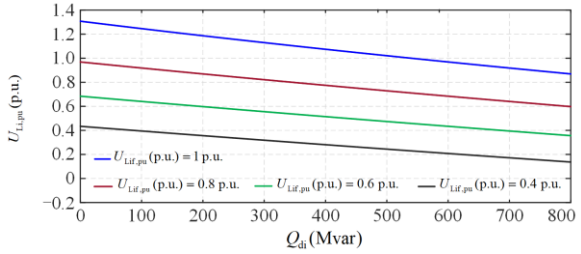

Fig. 8. The relationship between $U_{\mathrm{Li,pu}}$ and Q_{di} under different $U_{\mathrm{Lif,pu}}$.

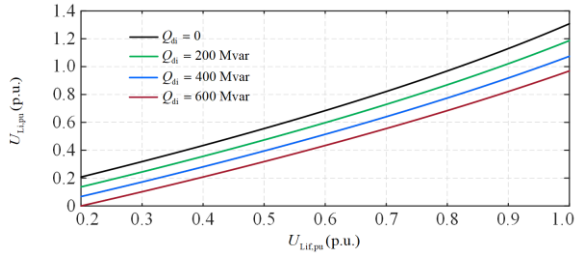

Fig. 9. The relationship between $U_{\mathrm{Li,pu}}$ and $U_{\mathrm{Lif,pu}}$ under different Q_{di}.

In Fig. 8 and Fig. 9, the increase of Q_{di} will lead to the decrease of $U_{\mathrm{Li,pu}}$, while the decrease of $U_{\mathrm{Lif,pu}}$ will cause $U_{\mathrm{Li,pu}}$ to decrease nonlinearly. It is indicated that Q_{di} will have a big influence on $U_{\mathrm{Li,pu}}$ for the serious fault. When a fault occurs, $U_{\mathrm{Lif,pu}}$ can be seen at a certain value, and in order to avoid $U_{\mathrm{Li,pu}}$ decreasing, from (8), Q_{di} can be controlled by I_{d} and U_{di}.

The short circuit ratio (S_{CR}) can be expressed as [33]:

$$S_{\mathrm{CR}} = \frac{S_{\mathrm{Ci}}}{P_{\mathrm{dN}}} \tag{18}$$

where P_{dN} is the rated DC power.

Combining (16) with (18), $U_{\mathrm{Li,pu}}$ is:

$$U_{\mathrm{Li,pu}} = -\sqrt{\left(\frac{S_{\mathrm{CR}} P_{\mathrm{dN}}}{2Q_{\mathrm{CiN}}}\right)^2 - \frac{S_{\mathrm{CR}} P_{\mathrm{dN}} U_{\mathrm{Lif,pu}}}{Q_{\mathrm{CiN}}} + \frac{Q_{\mathrm{aciN}} + Q_{\mathrm{di}}}{Q_{\mathrm{CiN}}}} + \frac{S_{\mathrm{CR}} P_{\mathrm{dN}}}{2Q_{\mathrm{CiN}}} \tag{19}$$

When $P_{\mathrm{dN}} = 1000$ MW, the relationship between $U_{\mathrm{Li,pu}}$ and S_{CR} with $U_{\mathrm{Lif,pu}} = 0.2$ p.u. and different Q_{di} is shown in Fig. 10.

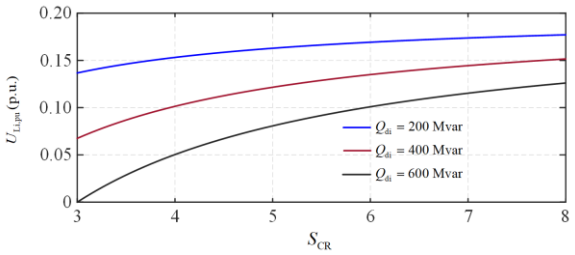

Fig. 10. The relationship between $U_{\mathrm{Li,pu}}$ and S_{CR} with different Q_{di}.

In Fig. 10, for a serious fault ($U_{\mathrm{Lif,pu}} = 0.2$ p.u.), with the decrease of S_{CR} (the AC system strength changes from strong to weak), the change of Q_{di} consumed by the inverter has a big effect on $U_{\mathrm{Li,pu}}$.

IV. Proposed Control Strategies

From (19), during the recovery process, $U_{\mathrm{Lif,pu}}$ can be calculated as:

$$U_{\mathrm{Lif,pu}} = \frac{S_{\mathrm{CR}} P_{\mathrm{dN}}}{4Q_{\mathrm{CiN}}} + \frac{Q_{\mathrm{aciN}} + Q_{\mathrm{di}}}{S_{\mathrm{CR}} P_{\mathrm{dN}}} - \left(U_{\mathrm{Li,pu}} - \frac{S_{\mathrm{CR}} P_{\mathrm{dN}}}{2Q_{\mathrm{CiN}}}\right)^2 \frac{Q_{\mathrm{CiN}}}{S_{\mathrm{CR}} P_{\mathrm{dN}}} \tag{20}$$

In (20), when $U_{\mathrm{Li,pu}} = U_{\mathrm{Lif,pu}}$, the maximum reactive power (Q_{dimax}) can be expressed as:

$$Q_{\mathrm{dimax}}=U_{\mathrm{Lif,pu}}S_{\mathrm{CR}}P_{\mathrm{dN}}+\left(U_{\mathrm{Lif,pu}}-\frac{S_{\mathrm{CR}}P_{\mathrm{dN}}}{2Q_{\mathrm{CiN}}}\right)^2Q_{\mathrm{CiN}}-\frac{(S_{\mathrm{CR}}P_{\mathrm{dN}})^2}{4Q_{\mathrm{CiN}}}-Q_{\mathrm{aciN}} \tag{21}$$

In (8), U_{di0} can be expressed as:

$$U_{\mathrm{di0}}=\frac{3\sqrt{2}}{\pi}NU_{\mathrm{Li,pu}}U_{\mathrm{LiN}} \tag{22}$$

Combining (8) with (22), $I_{\mathrm{dref,c}}$ (the DC current order calculation value) is:

$$I_{\mathrm{dref,c}}=\frac{\left[U_{\mathrm{Lif,pu}}S_{\mathrm{CR}}P_{\mathrm{dN}}+\left(U_{\mathrm{Lif,pu}}-\frac{S_{\mathrm{CR}}P_{\mathrm{dN}}}{2Q_{\mathrm{CiN}}}\right)^2Q_{\mathrm{CrN}}-\frac{(S_{\mathrm{CR}}P_{\mathrm{dN}})^2}{4Q_{\mathrm{CiN}}}-Q_{\mathrm{aciN}}\right]}{2\sqrt{\left(\frac{3\sqrt{2}}{\pi}NU_{\mathrm{Li,pu}}U_{\mathrm{LiN}}\right)^2-U_{\mathrm{di}}^2}} \tag{23}$$

From (3), when $\gamma=\gamma_0$ (extinction angle in normal operation state), the minimum converter bus voltage at the inverter side (U_{Limin}) can be calculated as:

$$U_{\mathrm{Limin}}=\frac{X_{\mathrm{ci,pu}}I_{\mathrm{d,pu}}}{\cos\gamma_0-\cos\beta} \tag{24}$$

For the HVDC system to recover quickly from the 1st CF, an AC voltage bias controller is designed as:

$$\Delta I_{\mathrm{dref}}=k_{\mathrm{i}}(U_{\mathrm{Lif,pu}}-U_{\mathrm{Limin}}) \tag{25}$$

where k_{i} is a fixed parameter, and $k_{\mathrm{i}}\geqslant 0$, so I_{dref} increases when $U_{\mathrm{Lif,pu}}>U_{\mathrm{Limin}}$, and decreases when $U_{\mathrm{Lif,pu}}<U_{\mathrm{Limin}}$.

From the above analysis, this paper proposes a subsequent commutation failure inhibition control strategy (SCFICS), as shown in Fig. 11.

As seen in Fig. 11, the proposed SCFICS consists of modules for AC fault voltage detection (FVDM), AC fault duration detection (FDDM), AC voltage bias control (VBCM), DC current reference calculation (CRCM). $I_{\mathrm{dref,V}}$ is the DC current value given by the VDCOL.

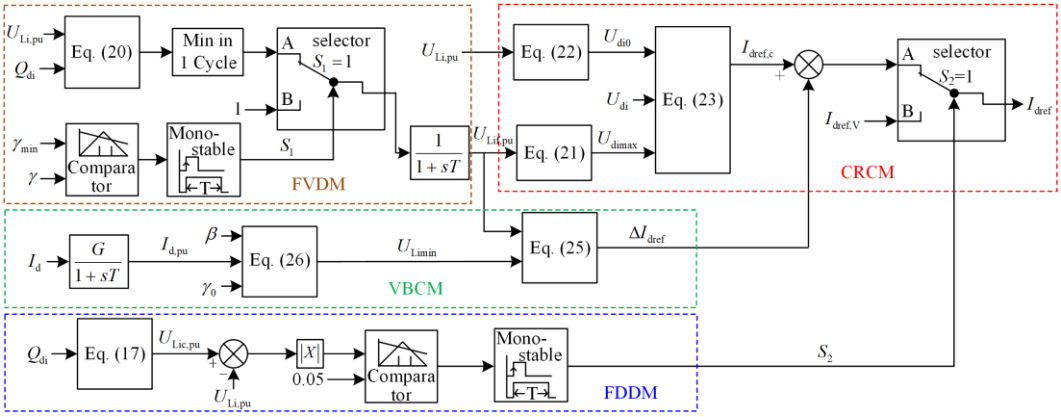

Fig. 11. The control block diagram of the proposed SCFICS.

The purpose of FVDM is to calculate $U_{\mathrm{Lif,pu}}$. By measuring Q_{di} and $U_{\mathrm{Li,pu}}$, based on (20), $U_{\mathrm{Lif,pu}}$ can be calculated. However, as $U_{\mathrm{Li,pu}}$ and Q_{di} will change dramatically, this may cause $U_{\mathrm{Lif,pu}}$ to have a large fluctuation. So to obtain a stable $U_{\mathrm{Lif,pu}}$, the minimum value of $U_{\mathrm{Lif,pu}}$ calculated by (20) during the 1st CF is taken as $U_{\mathrm{Lif,pu}}$.

The purpose of FDDM is to detect the fault duration. The main idea is that the fault duration has an obvious influence on the AC voltage (according to (16) and (17)), and hence, the error between $U_{\mathrm{Li,pu}}$ (calculated by (16)) and $U_{\mathrm{Lif,pu}}$ is compared and if it is bigger than a preset value (0.05 in Fig. 11), it implies that a fault has occurred in the AC system.

The main idea of VBCM is to improve the recovery time after the 1st CF. Considering the suppression of the SCF in (24), comparing U_{Limin} (calculated by (24)) and $U_{\mathrm{Lif,pu}}$ provides an error value (from (25)). Based on (21) and (23), by dynamically controlling the reactive power consumed by the inverter so as to keep the AC voltage at a stable value ($U_{\mathrm{Lif,pu}}$) during the whole AC fault duration, $I_{\mathrm{dref,c}}$ is obtained, and the final I_{dref} of the proposed control strategy can be expressed as:

$$I_{\mathrm{dref}}=I_{\mathrm{dref,c}}+\Delta I_{\mathrm{dref}} \tag{26}$$

As can be seen in Fig. 11, I_{dref} is dependent on the AC voltage, DC voltage and AC system strength, and these are the main reasons for an SCF. By controlling the reactive power consumed by the inverter, the effect of the coupling relationship among I_{d}, Q_{di} and β on extinction angle is decreased, so the proposed SCFICS can effectively inhibit the SCF.

V. Case Study

A. Comparison of Simulation Results between the Original System and SCFICS

Based on the SIEMENS control strategy (Fig. 2) and CIGRE HVDC Benchmark model parameters [35], the SCFICS is built in PSCAD/EMDTC.

In Fig. 11, the $\gamma_{\min}$ and γ_0 are 7° and 15°, respectively. The different cases are shown in Table II, and the serial number settings in the figures are shown in Table III, e.g., A1 represents the simulation results of γ in Case A.

Figures. 12 and 13 depict the simulation results based on Table II. Cases A, B and C have the same fault type (TPG) and fault duration ($t_{dur}=0.2$ s), with different fault inductances (L_f) of 0.1 H, 0.5 H and 0.9 H, respectively. By comparing the Cases B, C and E, the effect of different fault durations ($t_{dur}=0.2$ s, 0.1 s and 0.15 s, respectively) on the SCF can be clarified. Cases F, G and H indicate the performance of the proposed

TABLE II
Overview of the Simulation Cases

Cases	Fault types	L_f (H)	t_{dur} (s)	Figs.
A	TPG	0.1	0.2	12 (a)
B	TPG	0.5	0.2	12 (b)
C	TPG	0.9	0.2	12 (c)
D	TPG	0.5	0.1	12 (d)
E	TPG	0.5	0.15	13 (a)
F	SPG	0.2	0.2	13 (b)
G	SPG	0.5	0.2	13 (c)
H	SPG	0.8	0.2	13 (d)

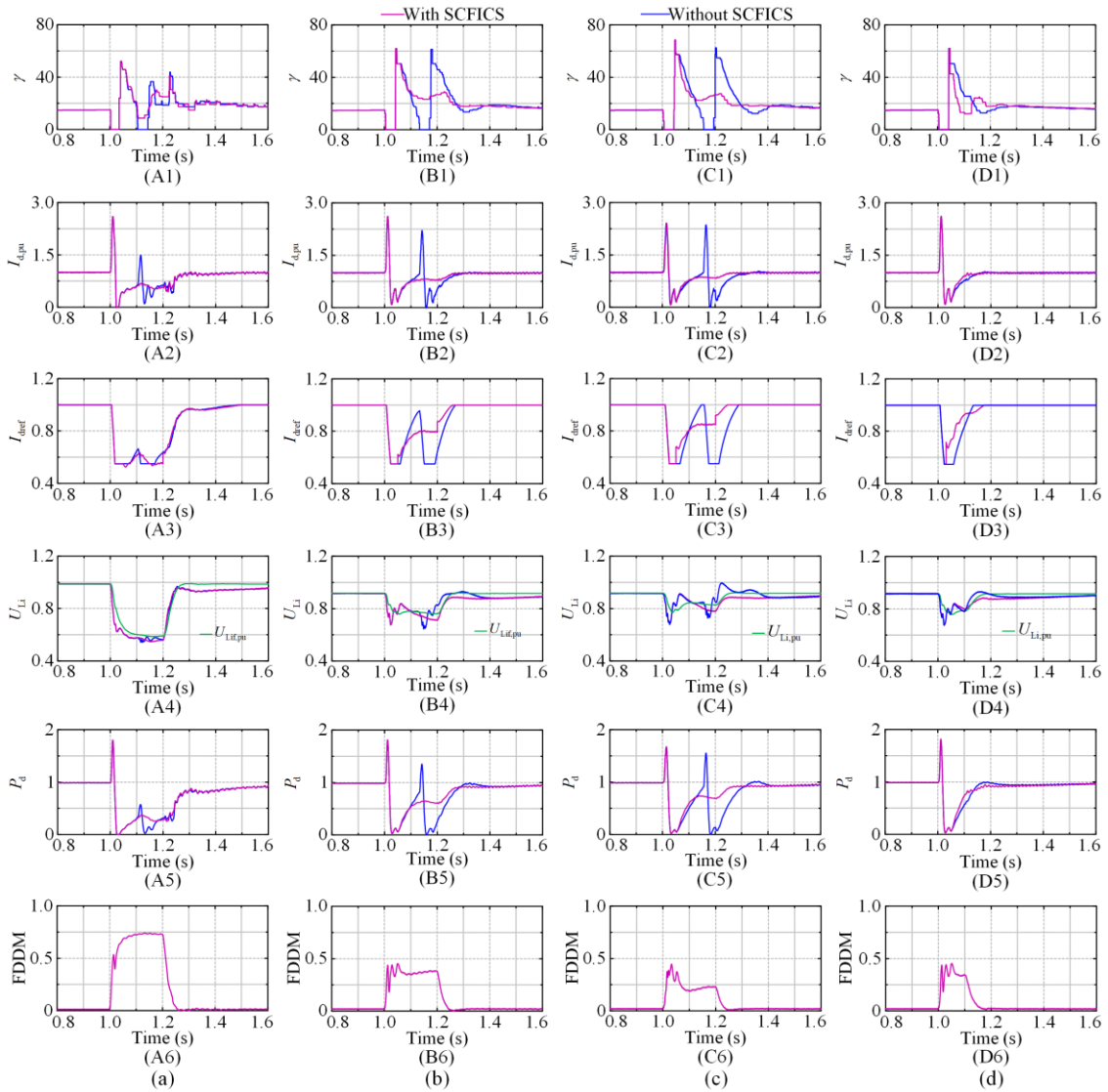

Fig. 12. The performance of the proposed control strategy in different cases. (a) Case A: A1–A6, TPG fault with $L_f=0.1$ H and $t_{dur}=0.2$ s. (b) Case B: B1–B6, TPG fault with $L_f=0.5$ H and $t_{dur}=0.2$ s. (c) Case C: C1–C6, TPG fault with $L_f=0.9$ H and $t_{dur}=0.2$ s. (d) Case D: TPG fault with $L_f=0.5$ H and $t_{dur}=0.2$ s.

control strategy by applying a single-phase-to-ground fault (SPG) with $t_{dur}=0.2$ s and $L_f=0.2$ H, 0.5 H and 0.8 H, respectively. For all cases, the proposed control strategy (SCFICS) shows good performance, i.e., when the SCFICS is not applied, all cases have SCF, whereas by applying the SCFICS, there is no SCF in any case.

TABLE III
THE SERIAL NUMBER SETTINGS IN THE FIGURES

Serial numbers	Setting	Serial numbers	Setting
1	γ	4	U_{Li}
2	$I_{d,pu}$	5	P_d
3	I_{dref}	6	FDDM

From the simulation results of γ in Figs. 13 (A1), (B1) and (C1), γ decreases to 0 twice, and an SCF occurs without applying the SCFICS. However, after applying the SCFICS, CF only occurs once (the 1st CF), and γ remains at a high value during the recovery process. With the increase of L_f, from the simulation results of γ and I_d, the time of the SCF is shifted backward. The DC current (I_d) and DC power (P_d) rise adaptively according to the change of the AC voltage (fault severity). This indicates that the proposed control strategy is beneficial to CF recovery.

For Case D, $t_{dur}=0.1$ s, as can be seen in Fig. 12 (D1), only the 1st CF occurs, although with the increase of t_{dur}, an SCF occurs for $t_{dur}=0.15$ s and 0.2 s. In contrast, there is no SCF occurrence in Case D after applying the SCFICS, while I_d has a noticeable rise during the recovery process, promoting rapid system recovery.

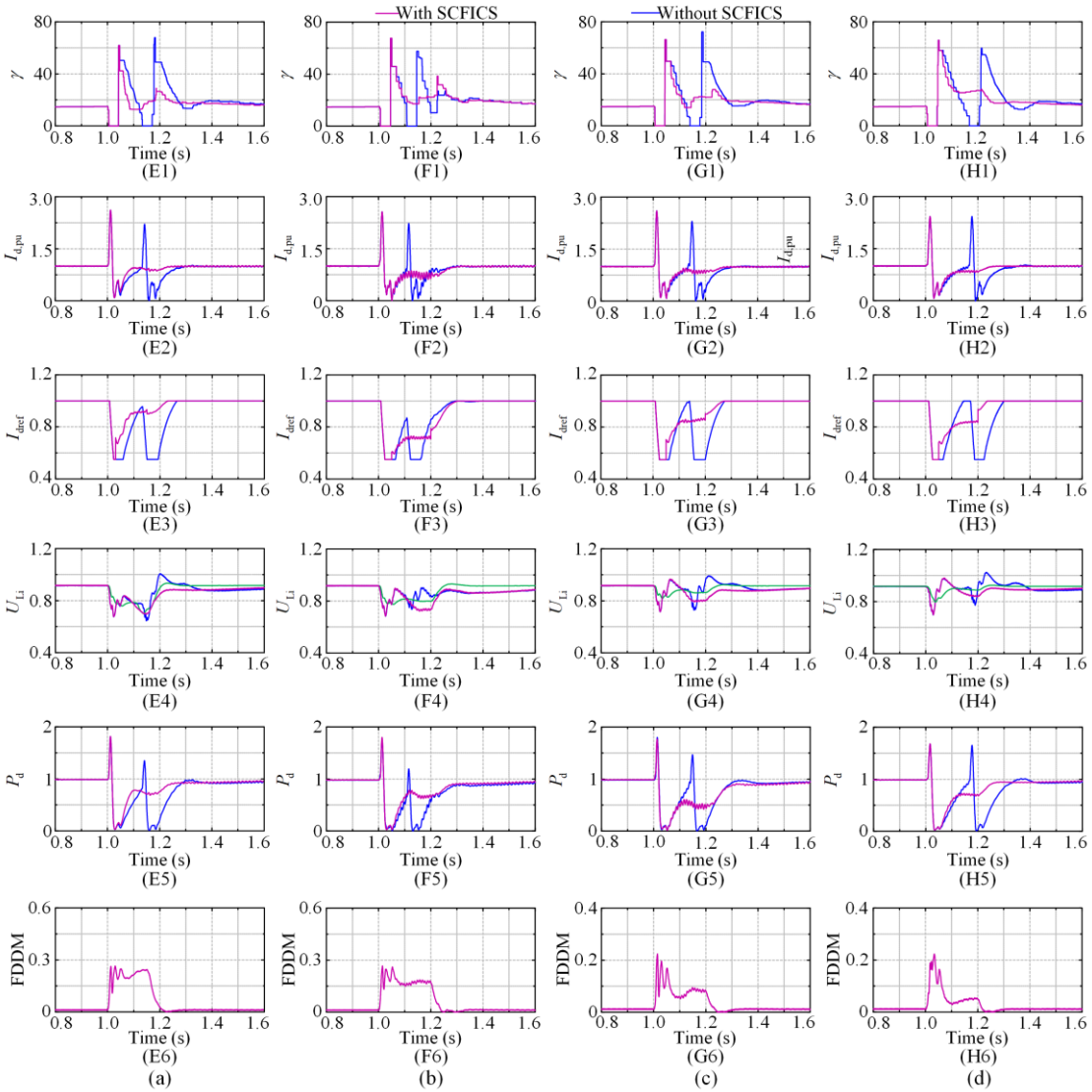

Fig. 13. The performance of the proposed control strategy in different cases. (a) Case E: E1–E6, TPG fault with $L_f=0.5$ H and $t_{dur}=0.15$ s. (b) Case F: F1–F6, SPG fault with $L_f=0.2$ H and $t_{dur}=0.2$ s. (c) Case G: G1–G6, SPG fault with $L_f=0.5$ H and $t_{dur}=0.2$ s. (d) Case H: H1–H6, SPG fault with $L_f=0.8$ H and $t_{dur}=0.2$ s.

For Cases A, B and C, sine the SCFICS has considered the fault severity, with the increase of L_f, I_{dref} also increases during the recovery process. In the early recovery period after the 1st CF, the SCFICS will output a lower I_{dref} than that of the original system. This can decrease the reactive power consumed by the inverter and maintain AC voltage at a high level. The lower I_d and higher U_{Li} are beneficial in resisting extinction angle decrease. In the later stage, after detecting the disappearance of the fault, the AC voltage will recover to the normal value, and hence, the SCFICS will output a higher I_{dref} than that of the original system to enhance the recovery speed.

For Cases F, G and H, the simulation results prove that the SCFICS has good performance with the SPG fault and different fault inductances. In all cases, regardless of the fault duration, the FDDM can output a high-level value during the fault. This indicates that the FDDM can effectively detect the fault duration. Within the fault duration, I_d can be controlled at a lower value based on the fault severity. This can effectively inhibit the SCF. After the AC fault, I_d can be controlled at a high value to improve system recovery.

The simulation results based on Table II validate that the SCFICS can effectively inhibit an SCF, and also shows a good recovery performance after the 1st CF.

Figure 14 depicts the performance of the SCFICS with different fault initiation times, fault types and fault inductances, with t_{dur} of 0.2 s. In Fig. 14 (a) and (b), from 0.01 H to 1 H, the fault initiation time is from 1 s to 1.09 s (half of one cycle). An SCF occurs in most cases when SCFICS is not applied. However, after applying the SCFICS, the SCF can be completely suppressed.

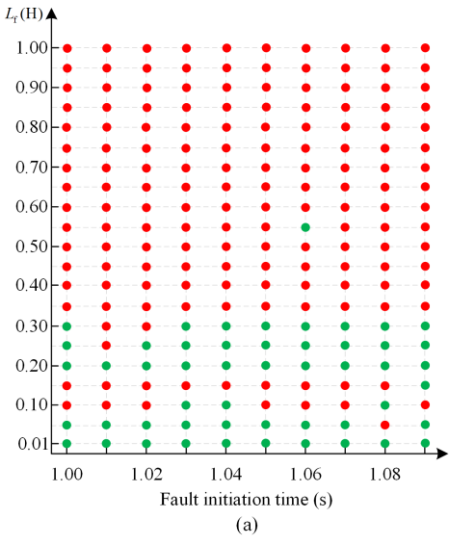

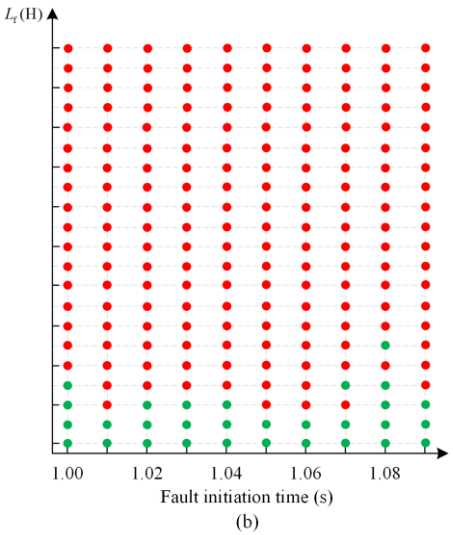

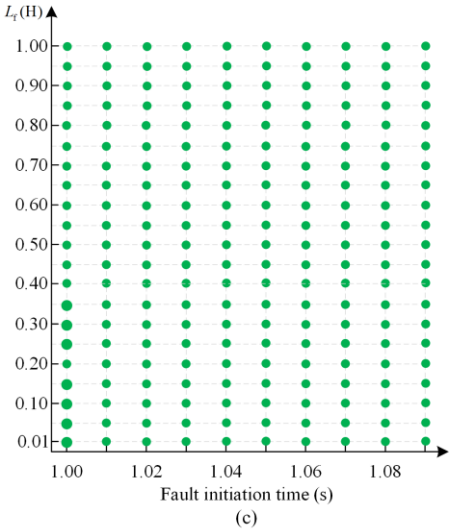

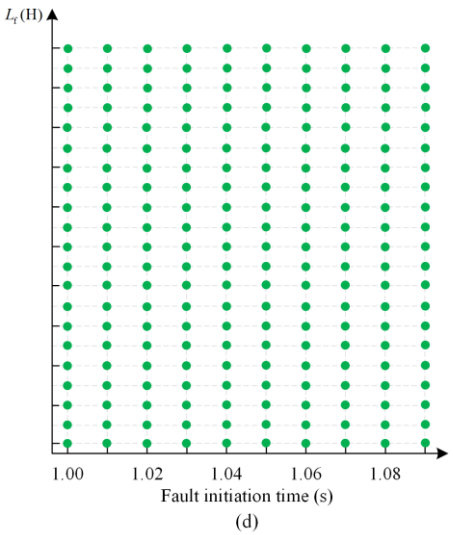

Fig. 14. The performance of the proposed strategy with different fault initiation times, different fault types and fault inductances. (a) TPG fault without SCFICS. (b) SPG fault without SCFICS. (c) TPG fault with SCFICS. (d) SPG fault with SCFICS.

B. Comparison of Simulation Results between the Existing Method and SCFICS

The performance of the SCFICS is compared with the current-limit control strategy in [17]. The case is set as: TPG fault ($L_f = 0.5$ H) and SPG fault ($L_f = 0.2$ H , respectively, t_f is 1.0 s, and t_{dur} is 0.2 s. The simulation results are shown in Fig. 15.

From Fig. 15(a), it can be seen that the SCFICS with TPG fault has a better performance with a larger extinction angle and converter bus voltage (U_{Li}) during fault recovery than that of the current-limit control strategy [17]. Fig. 15(b) also shows that P_d and U_{Li} after applying SCFICS with SPG are bigger than those from [17].

The current-limit control strategy in [17] cannot self-change based on the fault severity, and the coupling relationship between the extinction angle, I_d and U_{Li} is not considered. Even so it can also inhibit an SCF, but the SCFICS is more effective in improving system recovery speed.

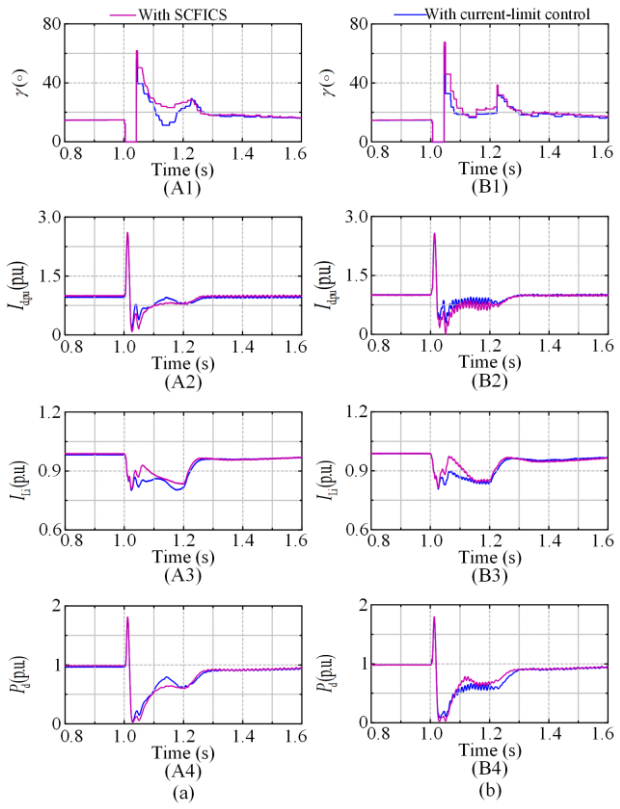

Fig. 15. The performance of the proposed strategy (SCFICS) and current-limit control strategy. (a) TPG fault with $L_f = 0.5$ H . (b) SPG fault with $L_f = 0.2$ H .

VI. Discussion

For an AC-DC hybrid system, the topological structure of the inverter, DC control strategy and AC system strength are key factors that affect steady-state and transient performance.

As shown in Fig. 2, during the transient period, the DC current control and extinction angle control have significant influence on the recovery process after the 1st CF. The SCFISCS proposed in this paper is to replace the DC control strategy of the original system after the 1st CF, and hence, the recovery performance is related to the SCFICS and not the DC system. Since the SCFICS is based on (21), which takes into account the impact of AC system strength (SCR), the proposed SCFICS can adapt to different AC/DC systems. For the same fault type and duration, the SCFICS will have a better performance than the existing approaches.

However, as (21) is based on [29] and the influence of the equivalent resistance of AC system and active power on transient voltage (ULi), when the LCC-HVDC is connected to a weak AC system (SCR is very small), the SCFICS proposed in this paper may have a different result.

In addition, the converter structure used in this article is a single LCC-HVDC, while for multi-infeed HVDCs, the interaction relationship between one inverter and another inverter will also impact on the SCFICS proposed in this paper.

VII. Conclusion

Given the problem of an SCF caused by AC system fault, this paper proposes a novel recovery strategy to suppress SCF in an LCC-HVDC, and the conclusions can be summarized as:

1) Based on the analysis of coupling relationship between extinction angle, AC voltage, firing angle and reactive power, it is concluded that there is a strong coupling relationship among them during the dynamic process, one which has a significant impact on an SCF.

2) Considering the reactive power interaction between the AC and DC systems, a mathematical expression of AC transient voltage is established, indicating that fault duration, fault severity and AC system strength are the main factors affecting SCF. Based on this, a novel recovery strategy to suppress SCF is proposed, one which can dynamically adjust the DC current order value.

3) Different from the commonly used control strategies, the SCFICS proposed in this paper can not only inhibit SCF more effectively, but also enhance the performance of system recovery.

4) In this paper, only the single LCC-HVDC system is used, while multi-infeed HVDCs and LCC-VSC hybrid systems have more complex reactive power interaction characteristics. How to extend the proposed control strategy to other systems needs further research.

5) The proposed transient voltage expression considering the fault duration and fault severity has universality, and can also be used in the sending-AC system transient voltage analysis.

APPENDIX A

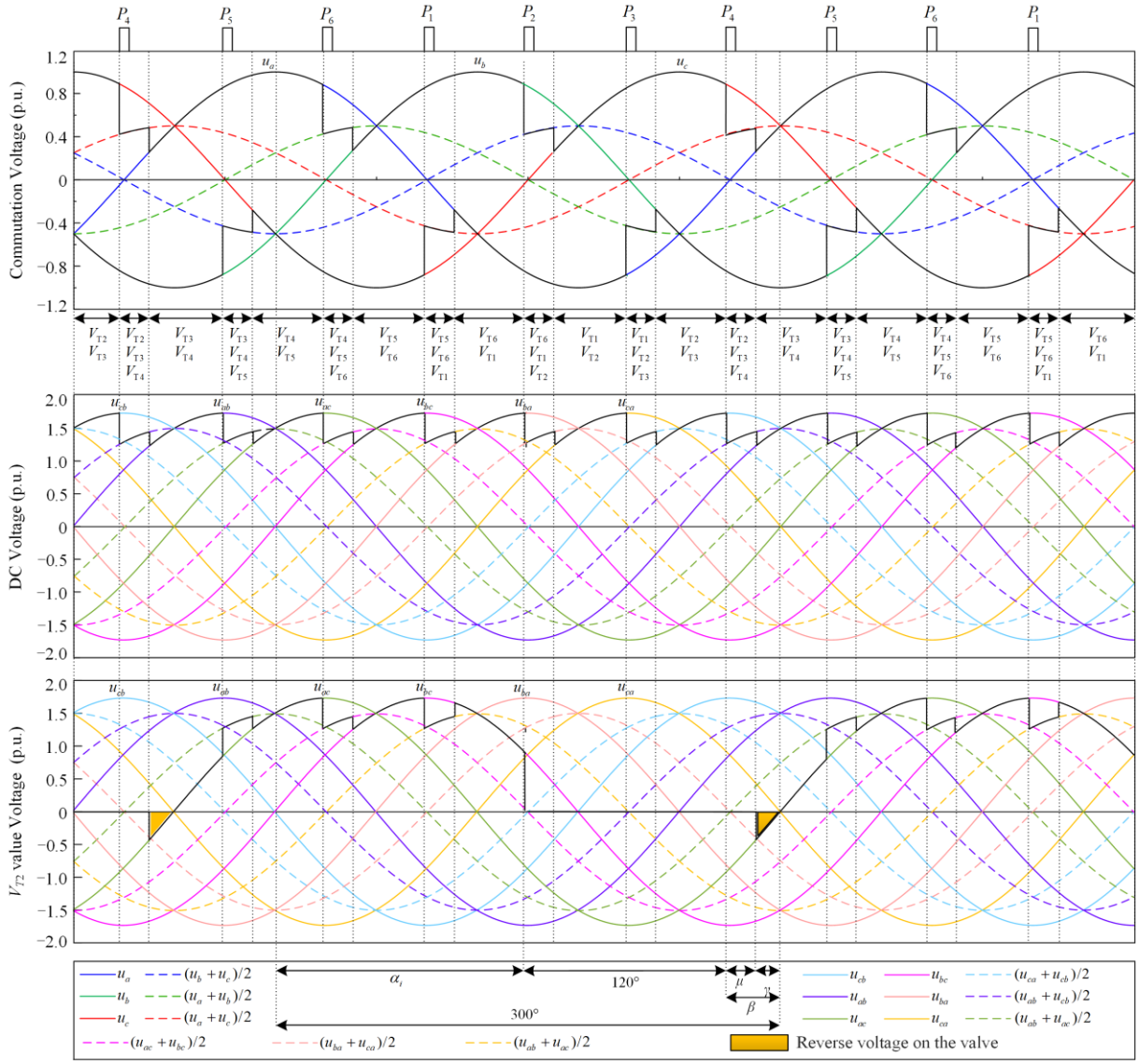

Fig.A1. Commutation voltage, DC voltage and valve voltage (V_{T2}) waveforms of a Graetz bridge during inverter model.

ACKNOWLEDGMENT

Not applicable.

AUTHORS' CONTRIBUTIONS

Changsheng Su: software, validation, formal analysis, investigation and writing. Chunya Yin: conceptualization, methodology, writing and project administration. Fengting Li: data curation. Lu Han: visualization. All authors read and approved the final manuscript.

FUNDING

This work is supported in part by the Natural Science Foundation of Xinjiang Uygur Autonomous Region, China (2022D01C85).

AVAILABILITY OF DATA AND MATERIALS

Not applicable.

DECLARATIONS

Competing interests: The authors declare that they have no known competing financial interests or personal relationships that could have appeared to influence the work reported in this article.

AUTHORS' INFORMATION

Changsheng Su received the B.S. degree and M.S. degree in power system and automation from the Xinjiang University, Urumqi, China, in 2009 and 2012, respectively. Currently, he is now mainly engaged in

research on stability and control of AC/DC hybrid power system.

Chunya Yin received the B.S. and Ph.D. degrees in electrical engineering from the School of Electrical Engineering of Xinjiang University, Urumqi， Xinjiang, China, in 2016 and 2021, respectively. He is an associate professor with the School of Electrical Engineering of Xinjiang University. His current research focuses on stability and control of ac or dc hybrid power system.

Fengting Li received the B.S. degree from the Beijing Institute of Technology, Beijing, China, in 1986, and the M.S. and Ph.D. degrees from Xinjiang University Urumqi, China, in 1996 and 2011 respectively. During 2008–2009, she was with Tsinghua University, Beijing, China, as a Western Light Visit Scholar. She is currently a professor with the School of Electrical Engineering, Xinjiang University. Her main research interests include power system protection power system optimization, and electric market.

Lu Han received the M.S. degrees in electrical engineering from the School of Electrical Engineering of Xinjiang University, Urumqi， Xinjiang, China, in 2017. She is a lecturer with the School of Electrical Engineering of Xinjiang University. Her current research focuses on stability and control of ac or dc hybrid power system.

REFERENCES

[1] X. Dong, E. Guan, and L. Jing *et al.*, "Simulation and analysis of cascading faults in hybrid AC/DC power grids," *International Journal of Electrical Power & Energy Systems*, vol. 115, Feb. 2020.

[2] J. Liu, F. Li, and C. Yin *et al.*, "Mechanism of and suppression strategy for transient voltage fluctuation in the commutator bus of a hybrid cascaded DC system caused by commutation failure," *Power System Protection and Control*, vol. 51, no. 20, pp. 36-46, Oct. 2023. (in Chinese)

[3] T. Li, T. Zhao, and M. Lü *et al.*, "The mechanism and solution of the anomalous commutation failure of multi-infeed HVDC transmission systems," *International Journal of Electrical Power & Energy Systems*, vol. 114, Jan. 2020.

[4] Y. Zhu, S. Zhang, and D. Liu *et al.*, "Prevention and mitigation of high-voltage direct current commutation failures: a review and future directions," *IET Generation Transmission & Distribution*, vol. 13, no. 24, pp. 5449-5456, Dec. 2019.

[5] J. Hou, G. Song, and Y. Fan, "Fault identification scheme for protection and adaptive reclosing in a hybrid multi-terminal HVDC system," *Protection and Control of Modern Power Systems*, vol. 8, no. 2, pp. 403-419, Jun. 2023.

[6] C. V. Thio, J. B. Davies, and K. L. Kent, "Commutation failures in HVDC transmission systems," *IEEE Transactions on Power Delivery*, vol. 11, no. 2, pp. 946-957, Apr. 1996.

[7] F. Wang, T. Liu, and X. Li, "Decreasing the frequency of HVDC commutation failures caused by harmonics," *IET Power Electrons*, vol. 10, no. 2, pp. 215-221, Feb. 2017.

[8] H. Lee, G. Son, and J. Yoo *et al.*, "Effect of a SFCL on commutation failure in a HVDC system," *IEEE Transactions on Applied Superconductivity*, vol. 23, no. 3, Jun. 2013.

[9] Z. Wei, Y. Yuan, and X. Lei *et al.*, "Direct-current predictive control strategy for inhibiting commutation failure in HVDC converter," *IEEE Transactions on Power Systems*, vol. 29, no. 5, pp. 2409-2417, Sept. 2014.

[10] J. Lee, U. A. Khan, and H. Lee *et al.*, "Mitigation of commutation failures in LCC-HVDC systems based on superconducting fault current limiters," *Physica C-Superconductivity and Its Applications*, vol. 530, pp. 160-163, Nov. 2016.

[11] B. Gao, K. Yuan, and P. Dong *et al.*, "Design of direct-current fuzzy controller for mitigating commutation failure in HVDC System," *Journal of Electrical Engineering & Technology*, vol. 13, no. 4, pp. 1450-1458, Jul. 2018.

[12] S. Mirsaeidi, X. Dong, and D. Tzelepis *et al.*, "A predictive control strategy for mitigation of commutation failure in LCC-based HVDC systems," *IEEE Transactions on Power Electronics*, vol. 34, no. 1, pp. 160-172, Jan. 2019.

[13] S. Mirsaeidi, X. Dong, and D. M. Said, "A fault current limiting approach for commutation failure prevention in LCC-HVDC transmission systems," *IEEE Transactions on Power Delivery*, vol. 34, no. 5, pp. 2018-2027, Oct. 2019.

[14] L. Liu, S. Lin, and K. Liao *et al.*, "Extinction angle predictive control strategy for commutation failure mitigation in HVDC systems considering voltage distortion," *IET Generation Transmission & Distribution*, vol. 13, no. 22, pp. 5171-5179, Nov. 2019.

[15] S. Mirsaeidi and X. Dong, "An enhanced strategy to inhibit commutation failure in line-commutated converters," *IEEE Transactions on Industrial Electronics*, vol. 67, no. 1, pp. 340-349, Jan. 2020.

[16] J. Wang, M. Huang, and C. Fu *et al.*, "A new recovery strategy of HVDC system during AC faults," *IEEE Transactions on Power Delivery*, vol. 34, no. 2, pp. 486-495, Apr. 2019.

[17] J. Ouyang, Z. Zhang, and M. Pang *et al.*, "Current-limit control method to prevent subsequent commutation failure of LCC-HVDC based on adaptive trigger voltage," *International Journal of Electrical Power & Energy Systems*, vol. 122, no. 5, Nov. 2020.

[18] L. Liu, S. Lin, and J. Liu *et al.*, "Analysis and prevention of subsequent commutation failures caused by improper inverter control interactions in HVDC systems," *IEEE Transactions on Power Delivery*, vol. 35, no. 6, pp. 2841-2852, Dec. 2020.

[19] J. Ouyang, Z. Zhang, and M. Li *et al.*, "A predictive method of LCC-HVDC continuous commutation failure based on threshold commutation voltage under grid fault," *IEEE Transactions on Power Systems*, vol. 36, no. 1, pp. 118-126, Jan. 2021.

[20] B. Liu, Z. Chen, and S. Yang *et al.*, "Research on methods of measuring extinction angle and measures to suppress repetitive commutation failures through equivalent DC input resistance," *International Journal of Electrical Power & Energy Systems*, vol. 133, Dec. 2021.

[21] D. Tian, X. Xiong, and C. Xiao, "Early warning and inhibition of HVDC subsequent commutation failure during recovery process under grid fault," *IEEE Transactions on Power Delivery*, vol. 36, no. 2, pp. 1051-1062, Apr. 2021.

[22] C. Zheng, Y. Tang, and W. Zhang *et al.*, "Current order-based emergency control strategy for subsequent commutation failure elimination in HVDC," *International Transactions on Electrical Energy Systems*, vol. 31, no. 9, Aug. 2021.

[23] L. Hong, X. Zhou, and Y. Liu *et al.*, "Analysis and improvement of the multiple controller interaction in LCC-HVDC for mitigating repetitive commutation failure," *IEEE Transactions on Power Delivery*, vol. 36, no. 4, pp. 1982-1991, Aug. 2021.

[24] Y. Wang, X. Li, and Z. Cai *et al.*, "Continuous commutation failure suppression method based on dynamic compensation of firing angle deviation," *International Journal of Electrical Power & Energy Systems*, vol. 147, May. 2023.

[25] D. Li, Y. Gao, and M. Sun, "A general self-adaptive DC current control of LCC-HVDC for eliminating subsequent commutation failure," *IEEE Transactions on Power Delivery*, vol. 38, no. 3, pp. 2232-2235, Jun. 2023.

[26] R. Zhu, X. Zhou, and S. Luo *et al.*, "DC current order optimization based strategy for recovery performance improvement of LCC-HVDC transmission systems," *Journal of Modern Power Systems and Clean Energy*, vol. 11, no. 3, pp. 1020-1026, May 2023.

[27] J. Liu, S. Lin, and W. Zhong *et al.*, "Improved identification method and fault current limiting strategy for commutation failure in LCC-HVDC," *Journal of Modern Power Systems and Clean Energy*, vol. 10, no. 6, pp. 1761-1772, Nov. 2022.

[28] J. Ouyang, X. Pan, and J. Ye *et al.*, "An improved prediction method of subsequent commutation failure of an LCC-HVDC considering sequential control response," *Protection and Control of Modern Power Systems*, vol. 8, no. 3, pp. 772-782, Sept. 2023.

[29] Y. Shao and Y. Tang, "Fast evaluation of commutation failure risk in multi-infeed HVDC systems," *IEEE Transactions on Power Systems*, vol. 33, no. 1, pp. 646-653, Jan. 2018.

[30] W. Yao, C. Liu, and J. Fang *et al.*, "Probabilistic analysis of commutation failure in LCC-HVDC system considering the CFPREV and the initial fault voltage angle," *IEEE Transactions on Power Delivery*, vol. 35, no. 2, pp. 715-724, Apr. 2020.

[31] C. Yin and F. Li, "Real-time calculation method of DC voltage and current to eliminate the influence of signal delay," *IEEE ACCESS*, vol. 8, pp. 157168-157176, Aug. 2020.

[32] Y. Qin, C. Yin, and Q. Duan *et al.*, "Research on transient voltage characteristics and support strategy under a fault occurred in the near-zone of HVDC sending system," *Power System Protection and Control*, vol. 51, no. 20, pp. 169-177, Sept. 2023. (in Chinese)

[33] C. Yin and F. Li, "Reactive power control strategy for inhibiting transient overvoltage caused by commutation failure," *IEEE Transactions on Power Systems*, vol. 36, no. 5, pp. 4764-4777, Sept. 2021.

[34] C. Yin and F. Li, "Analytical expression on transient overvoltage peak value of converter bus caused by DC faults," *IEEE Transactions on Power Systems*, vol. 36, no. 3, pp. 2741-2744, May. 2021.

[35] C. Yin and F. Li, "A novel evaluation method for the risk of simultaneous commutation failure in multi-infeed HVDC-systems that considers DC current rise," *International Journal of Electrical Power & Energy Systems*, vol. 131, Oct. 2021.